Ceramics International 43 (2017) 4562–4569

Contents lists available at ScienceDirect

Ceramics International

journal homepage: www.elsevier.com/locate/ceramint

Slag corrosion of alumina-magnesia-carbon refractory bricks: Experimental data and thermodynamic simulation

Vanesa Muñoz[a], Silvia Camelli[b], Analía G. Tomba Martinez[a,*]

[a] Instituto de Ciencia y Tecnología de Materiales (INTEMA) – CONICET/UNMdP, Av. Juan B. Justo 4302, 7600 Mar del Plata, Argentina
[b] Instituto Argentino de Siderurgia (IAS), Av. Central y 19 Oeste, 2900 San Nicolás, Argentina

ARTICLE INFO

Keywords:
Alumina-magnesia-carbon refractories
Slag corrosion
Crucible test
Thermodynamic simulation

ABSTRACT

Alumina-magnesia-carbon (AMC) bricks are used in steelmaking ladles, where they are part of the bottom and sidewalls working linings. These refractories can be corroded by liquid slag, especially during tapping and casting. In order to contribute with information regarding the reaction mechanisms and the formed phases when they are in contact with a molten slag, the slag corrosion at high temperatures of three AMC refractories is analyzed in this paper. A crucible test was performed at 1600 °C using an industrial basic slag, and the results were compared with those obtained in testing at 1450 °C. In addition, thermodynamic simulations of the slag-refractory contact were performed using FactSage software and a model which considers the global chemical composition of each refractory. Differences in the materials wear associated with differences in composition were predicted by the simulation. Other determining factors, such as microstructure and texture of the evaluated AMC refractories, were also discussed.

1. Introduction

Alumina-magnesia-carbon (Al_2O_3-MgO-C, AMC) refractory bricks are used in the metal line and the bottom of the working linings of steelmaking ladles [1–5]. Their application in the slag line is limited due their susceptibility to basic melt attack at high temperature [2]. However, depending on the logistics of the steelshop, AMC refractories can be corroded by liquid slag, especially during tapping and casting. Although some works have been reported on the corrosion of AMC refractories [6–9], information regarding the reaction mechanisms and the characterization of the formed phases in the refractories' microstructure at high temperatures is still rather limited.

The thermodynamic simulation of refractory corrosion by melts using commercial software packages (such as Thermocalc or Factsage) is a very powerful tool that can be used to explain and predict the mineralogical composition of the refractory-slag system and even corrosion wear [10,11]. There are several models available for slag corrosion simulation, which have been mainly applied to the study of castables, with each one trying to reproduce the practical conditions better each time [10–13]. For example, Luz et al. [10] introduced the saturation of slag by the refractory components and its chemical composition change after the reaction with the refractory in the simulation model. Once the thermodynamic model has proved to be adequate for describing a refractory-slag system, it can be used to predict the final equilibrium state for different experimental conditions (changes in temperature, slag or refractory compositions, for instance), thus reducing the number of expensive and time-consuming experimental tests. Of course, the model cannot consider all the factors involved in the corrosion process, especially those related to kinetic aspects. Nevertheless, the corrosion mechanism and main determining factors regarding corrosion behavior may be also inferred from thermodynamic simulation data [10,11].

This work deals the evaluation of the corrosion of three AMC refractories in contact with an industrial typical slag at 1600 °C, in air. The results are compared with experimental data obtained at 1450 °C which were previously reported and discussed [9]. In addition, the thermodynamic simulation of the refractory-slag system at both temperatures, 1450 and 1600 °C, is performed using a model which considers the overall chemical composition of the refractory and the liquid slag composition changes due to the interaction with the refractory. In order to point out the advantages of the thermodynamic analyses, and use it to explain corrosion behavior, the results of experimental corrosion crucible tests are also compared to the calculated ones.

* Corrsponding author.
E-mail address: agtomba@fi.mdp.edu.ar (A.G. Tomba Martinez).

http://dx.doi.org/10.1016/j.ceramint.2016.12.114
Received 9 August 2016; Received in revised form 22 December 2016; Accepted 22 December 2016
Available online 27 December 2016

Table 1
Composition and texture data of AMC refractories.

		AMC1	AMC2	AMC3
Main phases (wt %)	Corundum (Al_2O_3)	82.7 ± 0.3	57.6 ± 0.3	70.5 ± 0.3
	Periclase (MgO)	5.40 ± 0.02	27.0 ± 0.1	6.8 ± 0.1
Secondary phases (wt%)	Mullite ($3Al_2O_3.2SiO_2$)	–	–	8.6 ± 0.3
	Graphite (C)	1.7 ± 0.1	3.5 ± 0.1	3.0 ± 0.1
	Resin (C, O, H)	5.4 ± 0.1	5.6 ± 0.1	5.0 ± 0.1
	Aluminium (Al)	1.39 ± 0.02	1.37 ± 0.02	1.60 ± 0.02
Impurities (wt%)	Fe_2O_3, SiO_2, CaO, TiO_2[a]	3.4 ± 0.3	4.9 ± 0.3	4.5 ± 0.3
Apparent porosity (%)		6.7 ± 0.1	7.8 ± 0.5	4.0 ± 0.1
Permeability (m^3/Nw/s)[b]		0.013	0.015	0.008
Minimum pore diameter (μm)		0.060	0.055	0.003

[a] Impurities expressed as oxides with contents > 0.1 wt%; others impurities are: K_2O, P_2O_5, Cr_2O_3, MnO, ZrO_2, SrO, ZnO.
[b] For ΔP of 3 MPa; ΔP is the pressure drop when the gas used in the measurement (N_2) passes through the sample.

2. Experimental procedures

2.1. Materials

Three alumina-magnesia-carbon (Al_2O_3-MgO-C, AMC) commercial refractory bricks manufactured by the same supplier and labeled as AMC1, AMC2 and AMC3 were analyzed. The bricks have different MgO content and different raw materials as sources of alumina.

Bearing in mind the aim of this work, these materials were characterized using a vast group of analysis techniques: X-ray fluorescence (XRF), plasma emission spectroscopy (ICP-OES), gravimetry, X-ray diffraction (XRD), differential thermal and thermogravimetric analyses (DTA/TGA), reflection optical microscopy and scanning electron microscopy coupled with X-ray dispersive energy (SEM/EDS), measurements of density and porosity, Hg-intrusion porosimetry, dilatometric analysis and permanent linear change (PLC). The refractory characterization results have been previously reported [14], and the main data are summarized in Table 1.

From these analyses, it was determined that every refractory contains brown fused alumina (Ea) plus tabular alumina (Ta). AMC1 has a higher proportion of the last type of aggregate with respect to Ea aggregates, and with respect to Ta aggregates present in the other two materials as well. Furthermore, it was confirmed that only AMC3 possesses bauxite (with a mullite content estimated around 8–9 wt%), and that aluminium is used as an antioxidant in the three materials in similar proportions. The higher amount of sintered magnesia in AMC2 is distributed in the medium-fine fraction whereas this component is present only as fine particles in the matrix of AMC1 and AMC3.

Graphite, whose particles have a similar aspect ratio in the three materials, is present at a higher content in AMC2, but its flakes are the smallest. The amount of graphite in AMC3 is somewhat lower and its particles are the purest. Furthermore, the bricks contain a similar amount of resins as organic binders, although it was not possible to determine what kind of phenolic resin they are (novolaka or resol).

Regarding the texture, AMC2 has a larger amount of open pores, although they are similar in size to those of AMC1. Conversely to what could be expected considering the presence of bauxite as source of alumina in AMC3, which has rather higher porosity (10–15%) than the other two sources of alumina (tabular and fused aluminas, with porosities < 3%), this is the brick with the lowest values of open porosity, permeability and pore size. This fact was attributed to a better granulometric fractions packing which would lead to lower levels and sizes of inter-particle pores.

The tortuosity parameter (determined by the Hg-intrusion porosimetry) was ~ 2 for each AMC refractory.

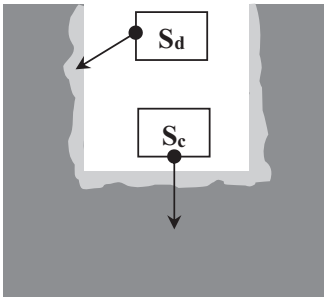

Fig. 1. Cross section of the corroded crucible.

2.2. Slag corrosion test

The corrosion behavior of AMC refractory bricks in contact with a typical ladle slag was studied at 1600 °C in air, employing the static crucible test. Crucibles of 6×6×5 cm^3 with a hole 3.6–3.7 cm in diameter and 2.3–2.5 cm in height, into which the slag in powder was placed, were used for the corrosion tests. These crucibles were thermally treated in an electric chamber furnace (SiC heating elements; Carbolite HTF 1700) at 1600 °C for 2 h. After the thermal treatment, the crucibles were cut transversally and then packed in epoxy resin in vacuum. The cross surfaces were ground with SiC papers up to 4000 grit of abrasive grade and polished with diamond paste up to 3 μm, using kerosene as a lubricant.

Corrosion was measured by the worn cross-area of the crucible (in percentage), which is a consequence of the irreversible loss of the refractory particles attacked by the slag. Photos were taken of the cross sections and the images were analyzed using Image Pro Plus 6.0 software. The new inner surface of the crucible was delimited on the cross section image and used to calculate the worn area S_d as a percentage of the original cross-area of the crucible, S_c (Fig. 1).

The slag used in the corrosion tests was that left in the ladle after the end of the continuous casting. It was characterized by several experimental techniques (XRF, XRD, DTA-TGA and critical temperature determination), and the results have been previously reported [9]. From the chemical composition (Table 2), the basicity index IB_2 (CaO/SiO_2 ratio) was calculated giving a value of 10.8, which indicates its basic character. The softening temperature of the slag was 1366 ± 5 °C, and its viscosity (η) at 1600 °C was estimated at 0.152 Pa s using the Urbain model [15], which has been extensively used to achieve a very good approximation of this property for steelmaking slags.

2.3. Thermodynamic simulation

The calculations performed in this work were based on the minimization of the free energy of the system in order to find out the chemical composition of the solid, liquid and gaseous phases, as well as their proportions at the thermodynamic equilibrium. Simulations have been carried out using FactSage (version 6.4), a fully integrated database and software developed between Thermfact/CRCT (Montreal) and GTT-Technologies (Aachen). The equilibrium phases, as well as the lowest temperature of liquid formation of the slag (equivalent to its melting point), were predicted using the Equilib module.

An iterative procedure which considers the liquid composition changes due to the brick corrosion [10] was used in the thermodynamic calculations. Firstly, 100 g of each AMC brick and 100 g of a slag composition (taking only those components ≥0.50 wt%) were considered in the first reaction stage. All calculations were performed for a constant temperature of 1450 or 1600 °C and a pressure of 1 atm. After the first reaction step, the resulting liquid (considered as the modified slag) was again put in contact with the same amount (100 g) of the original brick composition used before, and a further thermodynamic calculation step (CS) was carried out. This procedure was constantly

Table 2
Chemical analysis of slag (XRF).

	SiO_2	CaO	Al_2O_3	MgO	FeO	MnO	Cr_2O_3	S
wt%	5.040 ± 0.100	54.94 ± 0.600	30.833 ± 0.700	8.187 ± 0.290	0.374 ± 0.040	0.120 ± 0.002	0.015 ± 0.002	0.517 ± 0.006

repeated until no liquid was present at the equilibrium.

Since the three AMC bricks have nearly the same resin content and no data for organic compounds were available in the used FactSage software version, this component was dismissed in the calculations. For the AMC bricks' composition, only the main and secondary phases were taken into account (Table 1). However, in order to include the effect of the minor components of the bricks (see 'Impurities' in Table 1), these oxides were incorporated in the equilibrium calculation as part of the initial slag composition. Predictions of the phases contained in the bricks thermally treated at 1450 and 1600 °C (without slag present) were also performed using the FactSage software. Furthermore, the viscosities of liquids at the equilibrium were estimated using the Viscosity module.

3. Results and discussion

3.1. Slag corrosion tests

The results of the slag corrosion behavior analysis of the three AMC refractories at 1450 °C (2 h, in air) were reported in previous work by the authors [9]. Data obtained in corrosion tests at 1600 °C (2 h, in air) are now presented, in comparison with previous results at 1450 °C.

The cross sections of the crucibles after the corrosion tests at 1600 °C are shown in Fig. 2. Remnant slag can be seen in the corroded crucibles: a small amount in AMC1, quite less in AMC3, and even less in AMC2, where the slag almost penetrated the crucible completely. The extent of penetration into the crucible walls was much greater in AMC2 than in AMC1 and AMC3, similar to what happened in crucibles tested at 1450 °C. As was expected, penetration at this lower temperature was less (a larger amount of remnant slag).

The corrosion wear determined in the cross section of the crucibles was 6%, 20% and 10% for AMC1, AMC2 and AMC3, respectively. It could be observed that the complete decarburation was only superficial, and graphite is still present in the inner part of the corroded crucibles. Compared to the corrosion wear measured at 1450 °C (AMC1: 5%, AMC2: 12%, AMC3: 9%), a marked increase in material degradation occurred in AMC2 (67% higher), although wear in the other two materials was only slightly higher at 1600 °C.

The refractory-slag interfaces observed by SEM showed high degradation in the three AMC materials. Similar to what happened in the crucibles tested at 1450 °C, the elemental analysis by SEM/EDS could only be performed on the attacked aggregates but not on the matrix.

The different types of aggregates were identified to analyze the phases formed by reaction with the molten slag. In general, these particles showed an intense attack since detection of the boundary between the attacked particle and the new formed phases was difficult. Furthermore, clearly defined layers of new phases, such as CA_6, CA_2 or $MgAl_2O_4$, observed in samples corroded at 1450 °C, were not noticed in any of the different types of aggregates. Conversely, the new solids were mixed between them. As in the materials corroded at lower temperature, flakes of graphite could not be identified in the refractory-slag interfaces due to the high wear of the bonding phase.

SEM images of tabular alumina aggregates (Ta) of AMC1 and AMC3, together with the phases identified by EDS are shown in Fig. 3 (dotted line indicates the refractory-slag interface). This type of aggregate could not be identified in the worn region of AMC2. This fact shows that the tabular alumina in contact with the slag was completely dissolved, probably due to the smaller size of this raw material in this refractory [14], compared to that used in the formulation of AMC1 and AMC3.

In contrast to what happened in the attack of coarse tabular alumina particles at 1450 °C, the formation of CA_6 in the vicinity of the aggregate was not detected in AMC1. In AMC3, this phase (absent in the original refractory) was identified in the region of the aggregate that was penetrated by the melt, as well as MA spinel, indicating the significant advance of infiltration. In the reaction zone next to the particle, calcium aluminates with a lower content of Al_2O_3 such as CA_2 and CA were detected, which was attributed to the greater homogenization of the ion's concentration due to the lower liquid viscosity and higher mobility of the species (with respect to the test at 1450 °C). This process would avoid the increase in the amount of alumina around the aggregate, which was the cause for CA_6 crystallization when the corrosion test was performed at 1450 °C [9].

Also, spinel was detected in the reaction zone, although as isolated crystals in both AMC refractories; this could be associated with a lower concentration of Mg^{+2} due to the same reasons mentioned above, especially in AMC1, which showed a continuous layer of this phase when the corrosion test was performed at 1450 °C [9]. Based on their morphology, the spinel crystals precipitated from the melt. Gehlenite (C_2AS) was identified close to the surfaces of the particles in the case of AMC1, as was anorthite (CAS_2) in AMC3; the difference in the composition of the ternary phases was a product of the higher SiO_2 content present in AMC3 refractory.

Images of the fused brown alumina aggregates (Ea) corroded by the molten slag at 1600 °C are shown in Fig. 4 for the three AMC refractories. The phases identified in the reaction zone of the Ea aggregates were similar to those observed at 1450 °C, and in the attacked tabular alumina particles at 1600 °C. CA_6 was identified in the vicinity of Ea particles in each material, although the formation of layers was not evident; even in AMC1, CA_6 was detected in the infiltrated region of the particle along with higher levels of Na. In each case, the calcium hexaluminate appeared together with small amounts of spinel, highlighting the mix of phases mentioned above. The

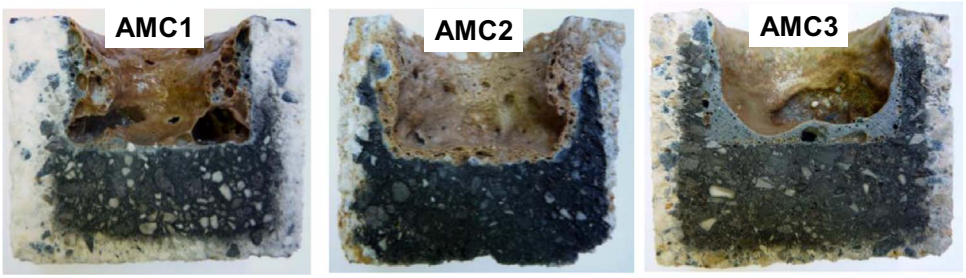

Fig. 2. Cross sections of crucibles after the corrosion tests at 1600 °C (2 h, in air).

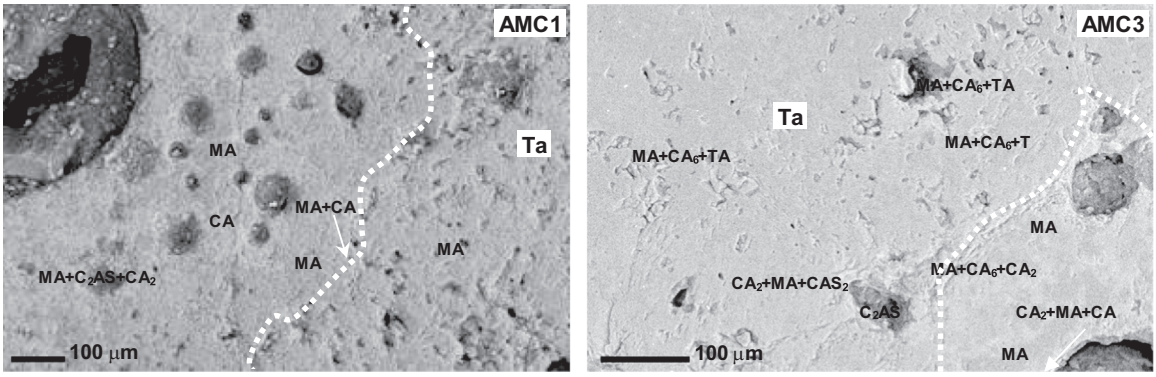

Fig. 3. Tabular alumina aggregates (Ta) corroded by the slag at 1600 °C (2 h, in air).

formation of spinel clusters near the corroded aggregate due to precipitation from the melt was only observed in AMC3. Although EDS points where only spinel was identified were also present in the other two materials, the crystals' morphology was less evident. Calcium aluminates with a lower content of Al_2O_3, such as CA_2, CA, $C_{12}A_7$ and C_3A, were detected far away from the alumina particles' surfaces.

As with what happened at 1450 °C, Ti-containing phases (Al_2TiO_5) were identified in AMC3 due to the high content of this element. Titanium came not only from the dissolution of the aggregate itself, which also occurs in AMC1 and AMC2, but also from bauxite, which has Ti-containing components as secondary phases. Aluminium titanate was identified along with the other already-mentioned phases. Towards the slag, CAS ternary phases such as anorthite and gehlenite were detected in AMC3 and AMC2, respectively, with a composition similar to that of anorthite in AMC1.

The bauxite aggregate (Bx) that was intensively attacked by slag, thus making it difficult to distinguish where the particle ends and

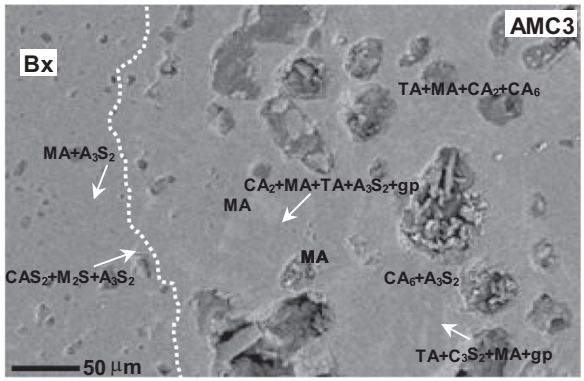

Fig. 5. Bauxite aggregate (Bx) attacked by the slag at 1600 °C (2 h, in air; gp: phase with high content of Si).

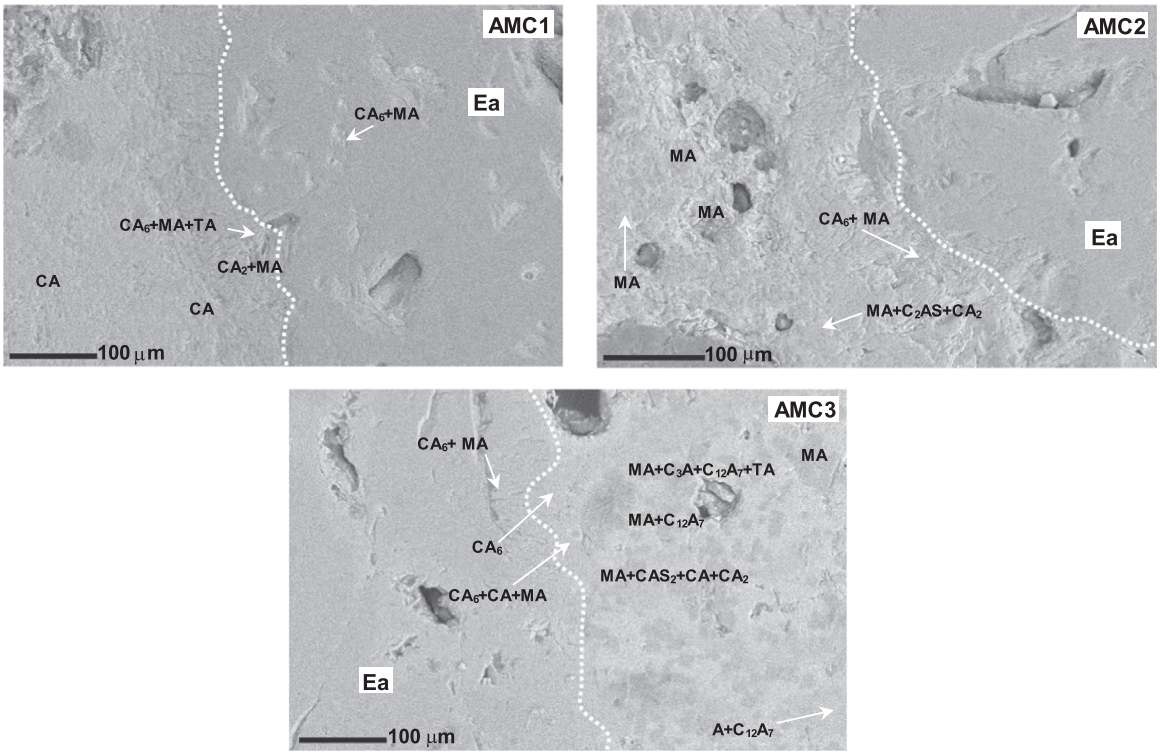

Fig. 4. Fused brown alumina aggregates (Ea) attacked by the slag at 1600 °C (2 h, in air).

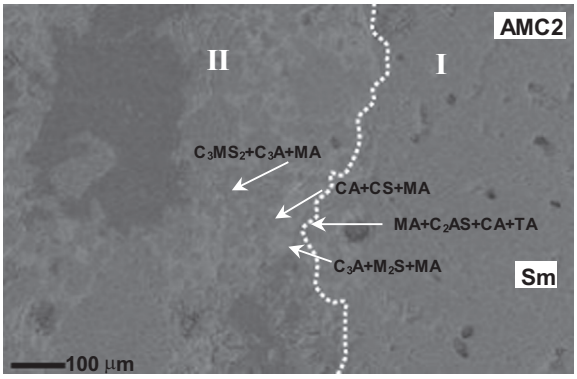

Fig. 6. Aggregate of sinter magnesia (Sm) attacked by the slag at 1600 °C (2 h, in air).

where the reaction zone begins, is shown in Fig. 5. Similar phases to those determined in the other type of alumina particles were identified, but their distributions were somewhat different. The calcium aluminates (especially CA_6) seems to be disseminated in different places, without a preferential localization alongside the aggregate boundary (in fact, defining this limit was difficult). These phases were detected in association with others like MA spinel, which was also observed isolated, and aluminium titanate. Zones enriched in Si were also observed and identified as possible glassy phase (gp) and mullite (A_3S_2), which could be either a relic of that present in the original bauxite aggregate or formed by dissolution and re-crystallization.

From the analysis of all these facts together, it was concluded that the analyzed zone is indeed a severely penetrated particle in which the slag infiltratrated through the grain boundaries with the help of Ti, which acted fluxing the liquid [17], and partially reacted without a complete dissolution of its components. Complete dissolution could actually occur in more peripheral layers of the aggregate. The intense attack displayed in this particle is in agreement with the literature, which recognizes the lower corrosion resistance of this type of raw material with respect to other alumina sources [8].

The chemical attack on the coarse magnesia particles in AMC2 was also aggressive, as is shown in the image in Fig. 6. Like that observed in the sample of AMC2 tested at 1450 °C, the attack to the periclase particle produced MA spinel, calcium aluminates with low Al_2O_3 content (CA and C_3A in this case, although in other reacted regions CA_2 and $C_{12}A_7$ were also identified), and binary and ternary silicon-containing phases (the proportion of Si increased locally due to the contribution of the sinter magnesia particle dissolution): calcium silicate (CS), forsterite (M_2S), merwinite (C_3MS_2).

Zones with distinct characteristics, labeled as I (next to the particle), II (intermediate) and III (next to the slag), were detected as a consequence of the slag attack on the MgO particle, analogous with those exhibited in the material tested at 1450 °C [9]. In the image shown below, only region I, corresponding to the penetrated aggregate, and the reacted zone II, which was thicker than that observed at 1450 °C, are observed. The texture of the formed spinel phase was

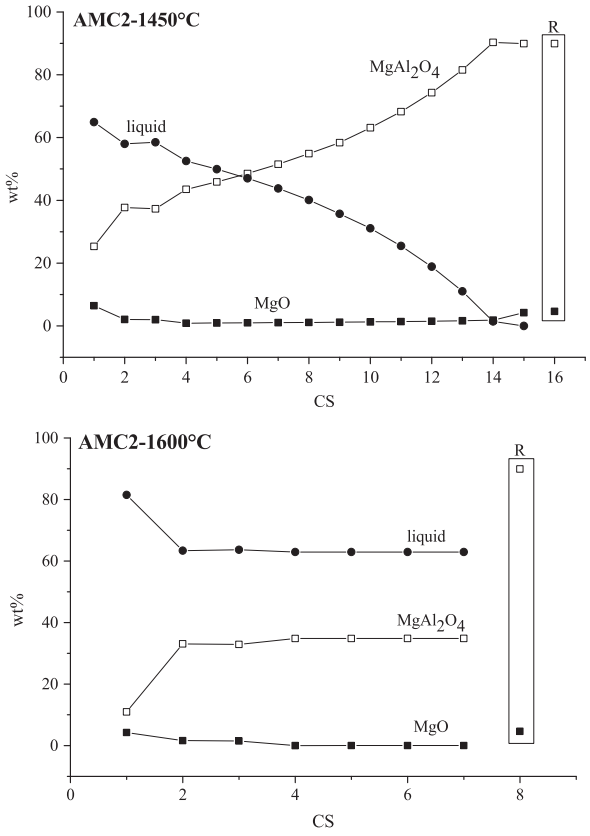

Fig. 7. Thermodynamic equilibrium phases at different the calculation steps (CS) in AMC2.

different from those crystals precipitated from the melt. The chemical degradation of periclase aggregates was clearly higher at 1600 °C than at 1450 °C.

A distinct aspect of the specimens tested at 1600 °C with respect to those tested at the lower temperature was the presence of regions whose EDS analyses revealed compositions close to CMA phases of the CaO-MgO-Al_2O_3 equilibrium diagram, such as $CaMg_2Al_{16}O_{27}$ (CM_2A_8, labeled as CMA-I) and $Ca_2Mg_2Al_{14}O_{28}$ (CMA_7, labeled as CMA-II) [18], in alumina as well as magnesia (in the case of AMC2) particles.

3.2. Thermodynamic simulation

The lower temperature at which liquid forms in the slag was estimated by calculation (considering only the components > 0.5 wt% in proportion) as 1304 °C, which is in agreement with the experimental value for the softening temperature. This ensures that the slag was fluid during the corrosion tests at 1450 and 1600 °C.

In the case of AMC1 and AMC3 materials, the simulation of the slag-refractory contact at 1450 °C required just two (2) calculation

Table 3
Proportion (in wt%) of the main equilibrium phases at 1450 °C in the original brick (R) and in contact with the slag (CS from 1 to 2).

		Al_2O_3	MA	Al_4C_3	G[a]	CA	CA_6	Melilite[b]	Liquid
AMC1	R	70.0	26.6	2.0	1.3	–	–	–	–
	CS=1	–	24.3	–	0.9	60.9	–	9.5	3.2
	CS=2	42.4	26.8	1.6	1.3	–	27.7	–	–
AMC3	R	60.0	34.8	2.4	2.8	–	–	–	–
	CS=1	–	26.3	–	1.6	50.0	–	12.3	8.1
	CS=2	2.0	31.6	1.4	2.4	–	64.0	–	–

[a] G: graphite.
[b] $Ca_2AlSi_2O_7$-$Ca_2Al_3O_7$.

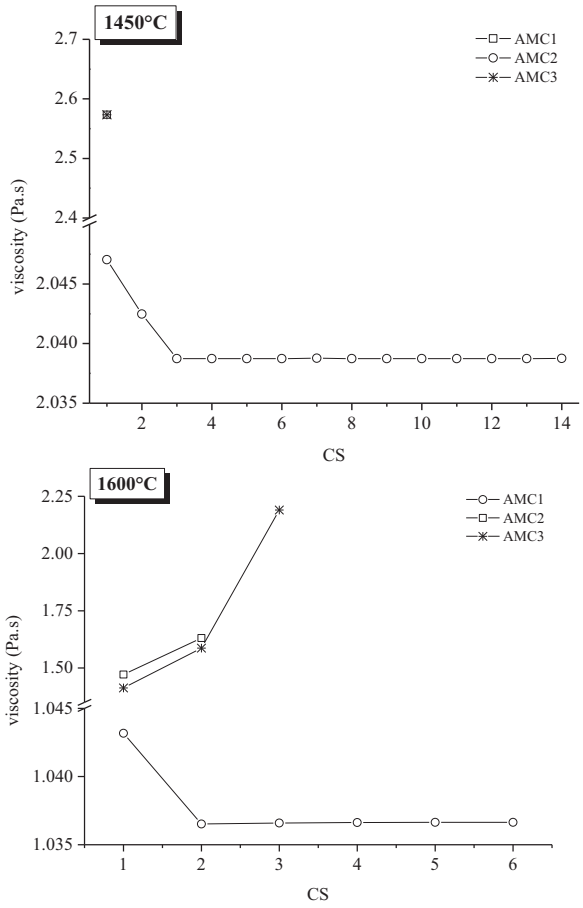

Fig. 8. Viscosity of equilibrium liquids at different calculation steps (1450 and 1600 °C).

steps (CS) for liquid to completely disappear as an equilibrium phase. For AMC2, the amount of liquid was zero only after fifteen (15) calculation steps.

The percentages of the main equilibrium phases at different calculation steps (CS) during the slag-refractory interaction at 1450 °C are reported in Table 3 (for AMC1 and AMC3) and Fig. 7 (for AMC2), together with the composition of the original materials (*R*) at the corrosion test temperature.

The minor phases calculated in the refractories in contact with the slag, most of them in percentages < 1.2 wt%, include: Fe_3C, FeSi, SiC and titanium carbide in the three materials, along with CaC_2 only in AMC2. The presence of phases such as Al_4C_3 and metal carbides (Fe, Si, Ti and Ca) is attributed to the fact that the simulation considers non-oxidant conditions, as gaseous O_2 was not incorporated into the system. As for $MgAl_2O_4$, it is stoichiometric in original refractories (*R*) and contains Fe in solid solution when in contact with the slag.

The viscosity calculated from the composition of the equilibrium liquids versus the calculation step is plotted for the three AMC refractories in Fig. 8.

The main equilibrium phases in the slag-refractory contact at 1600 °C are reported in Table 4 for AMC1 and AMC3. In these materials, the minor phases in thermodynamic equilibrium, all of them in contents < 1.0 wt%, were the same as those calculated at 1450 °C.

The proportion of major phases for AMC2 up to calculation step number seven (CS=7) is shown in Fig. 7. After this step, the program was not able to calculate the equilibrium composition, and the simulation had to be ended before the liquid amount was zero. The minor phases were the same present at 1450 °C, except for Ca_2C, which was absent at 1600 °C. As for the minor phases, only $Fe_{(l)}$ and SiC were calculated to be equilibrium phases in AMC2 at 1600 °C.

In the case of AMC2, the proportions of the equilibrium phases

Table 4
Proportion (in wt%) of the main equilibrium phases at 1600 °C in the original brick (R) and in contact with the slag (CS from 1 to 4).

		Al_2O_3	MA	Al_4C_3	G[a]	CA_2	CA_6	Liquid
AMC1	R	66.8	29.8	2.0	1.3	–	–	–
	CS=1	–	7.6	–	0.9	–	–	90.3
	CS=2	–	16.4	–	0.5	57.5	–	25.0
	CS=3	–	25.9	0.2	0.8	37.1	35.2	–
AMC3	R	55.9	38.9	2.4	2.8	–	–	–
	CS=1	–	10.7	–	1.6	–	–	86.1
	CS=2	–	17.7	–	1.0	45.9	–	34.6
	CS=3	–	29.5	–	1.4	52.2	13.9	1.9
	CS=4	39.7	46.0	2.0	2.7	–	9.2	–

[a] G: graphite.

varied very slowly after the third calculation step (CS=3), as can be observed in Fig. 7, with the difference between two consecutive calculation steps becoming smaller and smaller (for instance, < 0.05 g for the liquid). This could be one of the possible reasons why the software was not able to converge to the equilibrium composition. Even so, the evolution of phases in the AMC2-slag system is still useful for analyzing the refractory's behavior to corrosion. On one hand, since the composition's change from one step to the other was slight after calculation step number three (CS=3), it could be considered that the system almost reached equilibrium with the liquid at this stage. If this were the case, the liquid would be the major phase (> 60 wt%), which indicates severe degradation of the refractory. Another way to interpret the obtained results is to consider that, in the event that the phase contents maintain the same low rate of change after CS=3, nearly 100 calculation steps would be required to reach a negligible content of liquid.

Finally, the viscosity of liquids at the thermodynamic equilibrium for all of the refractories at 1600 °C are shown in Fig. 8 as the number of CS increases. The liquids in AMC2 and AMC3, which are very similar in composition, have almost the same increasing viscosities, although the values were slightly higher for AMC1.

3.3. Comparison between experimental data and thermodynamic simulation

Considering the total quantity of calculation steps (CS) to reach the thermodynamic equilibrium (i.e., when liquid content was zero) as a measurement of slag penetration [10] and in consequence, the corrosion of the refractory, the thermodynamic simulation appropriately anticipates the relative order of the extreme values of corrosion indicator determined at 1450 °C: the lowest value was for AMC1 (5% of wear index and remnant slag-low penetration [9]; total CS=2), with the highest for AMC2 (12% of wear index and low remnant slag-high penetration [9]; total CS=15). In the case of AMC3, the corrosion wear was higher (9% of wear index and remnant slag-low penetration) even though the number of calculation steps was equal to that of AMC1. In corrosion tests at 1600 °C, in agreement with an increase of the penetration and wear, a higher number of CS was required for liquid disappearance in AMC1 (6%, total CS=3) and AMC3 (9%, total CS=4). Taking into account the second interpretation of the AMC2-slag system simulation, a good correlation exists between the experimental corrosion indicator (22%) and the total number of CS (~100).

Bearing in mind that the simulation model used here only considered the chemical composition of the refractories, the contrast between AMC2 and the other two materials in relation to slag corrosion behavior should be caused by differences in the refractories' formulations, with the primary difference being the larger amount of MgO in AMC2. Based on the corrosion simulation, the high magnesia content has a negative impact on the corrosion resistance to the evaluated slag, in tune with that previously reported [7,8]. Besides the chemical

composition, other factors which could affect the experimental degradation of these AMC materials, such as the texture or the quality and size of the particles, were previously discussed [9].

Another factor provided by the thermodynamic calculation to justify the difference in the corrosion resistance of the studied AMC refractories is the amount of liquid present in the equilibrium condition. The simulation at 1450 °C predicted a proportion of liquid after the first calculation step of around 70 wt% for AMC2, which was the major phase, whereas the liquid amounts for the other two refractories were minor, ~8 wt% in AMC3 and even smaller in AMC1(~3 wt%). This difference in the liquid proportions between AMC1 and AMC3 could be one reason for the lesser wear observed in corroded crucible of the former. At 1600 °C, the initial amount of liquid (for CS=1) reached 80 wt% in AMC2, and then reduced to an almost constant quantity, but still elevated (> 60 wt%). In contrast to that calculated at 1450 °C, the liquid proportion in the other AMC refractories was almost the same as AMC2 in the first steps, but then decreased quickly, more so in AMC1, which would also explain its low corrosion wear.

On the other hand, the liquid viscosities during the interaction of AMC2 with the slag (Fig. 8) at 1450 °C and 1600 °C are always inferior to those calculated for AMC1 and AMC3, whose liquids are very similar. This favors the ability of the former melt to penetrate the material, as was observed in the corroded crucibles. At 1600 °C, the viscosity of all of the liquids decreased (Fig. 8). The small difference in the viscosity of liquids present in AMC1 and AMC3 at 1600 °C could contribute to the difference in the penetration observed in the corroded specimens.

The phases determined by SEM/EDS in AMC materials tested at 1450 °C have been previously reported [9]. In spite of the differences in morphologies and/or distributions, the formation of the following phases were detected in the three AMC materials: a) CA_6, CA_2 and CA calcium aluminates together with MA spinel and ternary CAS phases in the vicinity of alumina aggregates, and b) MA spinel and aluminates with a lower proportion of alumina, such as CA_2, $C_{12}A_7$, C_2A and C_3A, besides binary and ternary phases containing SiO_2, in the attacked particle of magnesia. Of these solids, MA spinel, CA and CA_6 are phases in thermodynamic equilibrium in the slag-AMC1 and slag-AMC3 systems based on the simulation (Table 3). Intermediate calcium aluminates are not predicted by thermodynamic simulation, although these solids were identified particularly in the slag region of corroded specimens. This fact highlights the restrictions imposed by kinetic factors that limit the species diffusion, mainly the Al^{+3} coming from the alumina particles' (Ta, Ea and bauxite in AMC3) dissolution. A surprisingly result is that calcium dialuminate is not an equilibrium solid, considering that it is the common intermediate phase between CA and CA_6, as was previously reported for others alumina-based systems [10], following the sequence: slag/CA//CA_2/CA_6/alumina aggregate. The formation of CA_2 and its conversion to CA_6 was proposed to occur by the reactions [10]:

$$2\ Al_2O_3\ (l) + CaO\ (l) \rightarrow CA_2(s)$$

$$CA_2(s) + 4Al_2O_3\ (l) \rightarrow CA_6\ (s)$$

where Al_2O_3(l) comes from the slag or the dissolved alumina particle. In fact, CA_2 was detected between these other calcium aluminates in the corroded AMC specimens [9]. It is considered that the absence of CA_2 as an equilibrium phase is a consequence of the limitations of the simulation model: in each of the calculation steps, the global system composition is different and, in terms of ternary phase diagrams for instance, it could move from one compatibility triangle to another one. In this way, the reaction sequence of calcium aluminates could be altered.

The only equilibrium phase present in AMC2 corroded samples was MA spinel. In this material, the high concentration of MgO moves the system composition toward the primary phase field of spinel [18]. The presence of calcium aluminates, none of them being compatible phases in thermodynamic equilibrium, is attributed to kinetic restrictions; near the alumina (tabular and Ea) and magnesia particles, the concentration of Al_2O_3 increased locally due to limited ion diffusion, leading to the formation of the calcium aluminates. This local system is displaced to the region of high alumina where the primary crystallization fields of these solids are located [18].

CA_2, CA_6 and MA spinel solids, foreseen as equilibrium phases in AMC1 and AMC3 at 1600 °C, were indeed identified in the corroded specimens. In the case of AMC2 at 1600 °C, as in the corrosion test at 1450 °C, only MA spinel identified by SEM/EDS was a solid present in the thermodynamic equilibrium of the refractory-slag system. The other calcium aluminates detected in specimens after the corrosion tests, especially towards the slag region, owe their presence to limited diffusion (kinetic factor), in spite of the higher temperature which favored ion diffusion.

Based on the above, the minor phases predicted by the thermodynamic simulation for AMC refractories were not detected by SEM/EDS. Carbides were not identified in the attacked regions, and Ti was mainly detected as part of aluminium titanate or as oxides. This was attributed to the fact that the conditions of the corrosion tests were more oxidant than those used in the equilibrium calculation.

Even the thermodynamic simulation predicted an increase in corrosion wear of the AMC refractories when temperature rose from 1450 to 1600 °C, more significant in AMC2 than in AMC1 and AMC3, the experimental results for the last two materials are surprising at first sight due their small variation. It is possible that there were other factors besides those taken into consideration in the thermodynamic simulation performed here (for example, the granulometric aspect) that could influence the corrosion behavior of AMC1 and AMC3.

There are signs that the slag's penetration into the three AMC refractory crucibles was indeed higher at 1600 °C than at 1450 °C. Bearing in mind that corrosion begins with an attack to the bonding phase, it is feasible to consider that the contribution of ions from this source would favour the early saturation of the melt, thus reducing the "necessity" to attack the aggregates, especially when *in situ* fine spinel was present in the matrix, because it can be easily attacked. Such would be the case of AMC1, where the spinel formation was more intensive, as previously reported [14], contributing to reducing the wear of this material at 1600 °C when compared to that determined at 1450 °C.

On the other hand, although an increase in the open porosity was determined in the three AMC refractories when temperatures increased, as reported in previous works of the authors [9,19], AMC3 retained smaller apparent porosity values, and even these parameters decreased at temperatures close to 1400 °C. This fact could improve AMC3 corrosion resistance, along with the spinel formation that occurred more slowly than in AMC1 [14].

In contrast with the other two refractories, the formation of *in situ* spinel occurred to a lower degree in AMC2, even with a quite higher proportion of MgO, and its apparent porosity increased continuously at high temperatures, always maintaining the highest values [9,19]. In consequence, these factors could not have had a positive effect of the corrosion resistance of AMC2, hence the increase of the corrosion indicator by a factor of two between 1600 °C and 1450 °C.

Even with restrictions, the simulation model used in this work gives several explanations to the corrosion behavior of the studied AMC bricks. This fact gives support for using the model to anticipate the corrosion response of these materials in other experimental conditions and also the effect of changes in the refractory and/or slag compositions on the corrosion behavior, avoiding experimental laboratory tests. One the other hand, the next planed improvements of the model is to incorporate the air atmosphere and to simulate the attack to the matrix and aggregates separately [13], although the last strategy needs further analysis to determine the chemical composition of each one, the bonding phase and the coarse particles.

4. Conclusions

The laboratory evaluation of the corrosion of AMC refractory bricks with different contents of sinter magnesia and alumina sources—AMC1, AMC2 and AMC3—enabled significant differences in material wear to be determined, even though the final phases analyzed by SEM/EDS were similar in the three cases. Moreover, a slight reduction in corrosion resistance from 1450 to 1600 °C was exhibited in AMC1 and AMC3 in contrast to what was expected. Nevertheless, the decrease of corrosion resistance was significant in AMC2.

The thermodynamic simulation of corrosion that employs a model based on the global chemical composition of the refractory and the slag and that considers the change in the melt composition caused by the refractory's dissolution, gave results that correlated rather well with the experimental data regarding penetration and wear, especially at 1600 °C. At this thermal condition, the systems should be approaching equilibrium due to higher ion mobility due to the presence of a greater amount of low viscous liquid. Furthermore, the solids identified by SEM/EDS in the corroded samples were similar to the equilibrium phases, even when the incidence of the kinetic factor was noted, especially at the lowest testing temperature.

Clearly, the model used for the corrosion simulation displayed good predictive and explicative power regarding the behavior of very complex materials as those in this work. Nevertheless, improvements to the simulation model by incorporating the atmospheric air present during corrosion and the differences in composition between the matrix and the aggregates are now being explored.

Acknowledgements

This work was carried out under research projects founded by the National Agency for Scientific and Technological Promotion (Agencia Nacional de Promoción Científica y Tecnológica, ANPCyT): PICT 2006 N°1887 “Thermochemical and thermomechanical degradation of oxide-C refractories of steelmaking use” and PICT 2012 N°1215 “Chemical degradation of refractory materials of steelmaking use”. The authors also thank to Dr. E. Brandaleze for the possibility of using the FactSage software.

References

[1] R. Koley, K. Rao, S. Askar, S. Srivastava, Development and application of Al_2O_3-MgO-C refractory for secondary refining ladle, in: Proceedings of the Unified International Technical Conference on Refractories UNITECR'01, 2001.

[2] S. Chatterjee, R. Eswaran, Optimization of slag corrosion resistance and thermal expansion in Al_2O_3-MgO-C brick, in: Proceedings of the Unified International Technical Conference on Refractories UNITECR'09, 2009.

[3] Y. Sasajima, T. Yoshida, S. Hayama, Effect of composition and magnesia particle size in alumina-magnesia-carbon refractories, in: Proceedings of the Unified International Technical Conference on Refractories UNITECR'89,.1989, pp. 586–603.

[4] A. Watanabe, H. Takahashi, S. Takanaga, N. Goto, O. Matsuura, S. Yoshida, Thermal and mechanical properties of Al_2O_3-MgO- C bricks, Taikabutsu Overseas 10 (3) (1990) 137–147.

[5] A.D. Gupta, K. Vickram, Development of resin-bonded alumina-magnesia-carbon bricks for steel ladle applications, Interceram 48 (5) (1999) 307–310.

[6] M. Kamiide, S. Yamamoto, K. Yamamoto, K. Nakahara, N. Kido, Damage of Al_2O_3-MgO-C brick for ladle furnace, J. Tech. Assoc. Refract. Jpn. 21 (4) (2001) 252–257.

[7] W.S. Resende, R.M. Stoll, S.M. Justus, R.M. Andrade, E. Longo, J.B. Baldo, E.R. Leite, C.A. Paskocimas, L.E.B. Sledade, J.E. Gomes, J.A. Varela, Key features of alumina/magnesia/graphite refractories for steel ladle lining, J. Eur. Ceram. Soc. 20 (2000) 1419–1427.

[8] J. Pötschke, T. Deinet, G. Routschka, R. Simmat, Properties and corrosion of AMC-refractories, Part II: corrosion by steel/slag, in: Proceedings of the Unified International Technical Conference on Refractories UNITECR'03, 2003, pp. 584–587.

[9] V. Muñoz, P.G. Galliano, E. Brandaleze, A.G. Tomba Martinez, Chemical degradation of commercial Al_2O_3-MgO-C refractory bricks by air and basic slag, J. Eur. Ceram. Soc. 35 (2015) 1621–1635.

[10] A.P. Luz, A.G. Tomba Martinez, M.A.L. Braulio, V.C. Pandolfelli, Thermodynamic evaluation of spinel containing refractory castables corrosion by secondary metallurgy slag, Ceram. Int. 37 (2011) 1191–1201.

[11] M.A.L. Braulio, A.P. Luz, A.G. Tomba Martinez, V.C. Pandolfelli, The role of CA_6 in the corrosion of cement-bonded spinel refractory castables: an analysis based on thermodynamic simulation, Ceram. Int. 41 (2015) 472–4714.

[12] J. Berjonneau, P. Pringent, J. Poirier, The development of a thermodynamic model for Al_2O_3-MgO refractory castable corrosion by secondary metallurgy steel ladle slags, Ceram. Int. 35 (2009) 623–635.

[13] A.P. Luz, M.A.L. Braulio, A.G. Tomba Martinez, V.C. Pandolfelli, Thermodynamic simulation models for predicting Al_2O_3-MgO castable chemical corrosion, Ceram. Int. 37 (2011) 3109–3116.

[14] V. Muñoz, P. Pena, A.G. Tomba Martinez, Physical, chemical and thermal characterization of Al_2O_3-MgO-C refractories, Ceram. Int. 40 (2014) 9133–9149.

[15] G.J. Browning, G.W. Bryant, H.J. Hurst, J.A. Lucas, T.F. Wall, An empirical method for the prediction of coal ash slag viscosity, Energy Fuels 17 (3) (2003) 731–737.

[17] H. Sarpoolaky, S. Zhang, B.B. Argent, W.E. Lee, Influence of grain phase on slag corrosion of low-cement castable refractories, J. Am. Ceram. Soc. 84 (2) (2001) 426–434.

[18] A.H. De Aza, J.E. Iglesias, P. Pena, S. De Aza, Ternary system Al_2O_3-MgO-CaO: part II, phase relationships in the subsystem Al_2O_3-$MgAl_2O_4$-$CaAl_4O_7$, J. Am. Ceram. Soc. 83 (4) (2000) 919–927.

[19] V. Muñoz, A.G. Tomba Martinez, Thermomechanical degradation of Al_2O_3-MgO-C refractory bricks under non-oxidising atmosphere, Ceram. Int. 41 (2015) 3438–3448.